

# Wind Loads on Utility Scale Solar PV Power Plants

**Joseph H. Cain, P.E., Principal Civil Engineer**  
**SunEdison**  
**Belmont, California**

**David Banks, PhD, P.Eng., Principal**  
**Cermak Peterka Petersen (CPP Wind)**  
**Fort Collins, Colorado**

## Abstract

The Solar Photovoltaic (PV) industry is experiencing phenomenal growth. Wind loads for ground-mounted PV power plants are often developed by using static pressure coefficients from wind tunnel studies in calculation methods found in ASCE 7. Structural failures of utility scale PV plants are rare events, but some failures have been observed in code-compliant structures.

Many wind loading codes and standards define flexible structures as slender structures that have a fundamental natural frequency less than 1 Hz. This paper demonstrates that this is not a suitable threshold for small structures like ground-mounted arrays of photovoltaic panels because structures this small can experience both self-excitation and buffeting from upwind panels at frequencies well above this value during both serviceability and design wind events.

## Introduction

This paper focuses on dynamic effects of wind for large-scale (often referred to as “utility scale”) solar photovoltaic power plants, and can be applied to most ground-mounted PV systems with repetitive rows of solar panels. This topic has relevance increasing in time as the solar industry scales in size and deployment, while continuously striving to drive down cost.

Solar market trends have been studied and the results published by GTM Research (a division of Greentech Media) and the Solar Energy Industries Association (SEIA). In Figure 1, from *U.S. Solar Market Insight 2014 Year-in-Review*, the blue bars show the phenomenal growth of the U.S. solar industry from 2005 through 2014. Market forecasts for the next two years are for 12 GigaWatts (GWdc) of installed capacity by the end of 2016. The Federal Investment Tax Credit (ITC) has been a driving force in attracting investors to kick-start the growth of the solar industry in the U.S. As the ITC and other incentive programs are expected to sunset, the solar industry is keenly focused on driving down

the installed cost of PV systems, with a goal of grid parity without incentives. The descending line in Figure 1 shows the trend in decrease of system price from 2005 to 2014.

Most of the reduction of system price has been a sharp decline in the cost of the power-producing PV modules (panels) themselves. As the cost of modules has decreased dramatically, a great deal of emphasis has been placed on *soft cost* (the cost of engineering and permitting) and *Balance of System (BOS)* cost, including the cost of the rack mounting system and foundation (but excluding inverters).

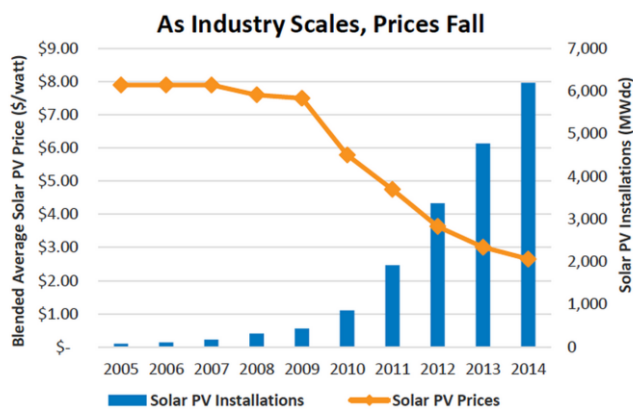


**Figure 1: Growth and price trends from 2005 to 2014**

As design engineers have strived to drive down the cost of the rack systems, many manufacturers have engaged wind consultants to model their systems in boundary layer wind tunnels. The products of these studies include more-accurate wind pressure coefficients to be used with procedures in ASCE 7. Economy of design has commonly included optimizing a reduction of steel, with a resulting trend toward structures that are more flexible. Structural failures have been observed in code-compliant ground-mounted rack systems during wind events at wind speeds significantly less than design wind speed. Recent research has been focused on determining the cause of failure in otherwise code-compliant structures and improving estimation of wind loads.

## Terminology

To facilitate the reader's understanding of terminology used in this paper, we offer the following introduction. Although *module* is actually an electrical term, the power-producing components that produce electricity from sunlight are often interchangeably referred to as *panels* or *modules*. Most solar modules have an extruded aluminum frame, but there are also double-laminated glass-on-glass modules that are frameless.

*Fixed-tilt* racks usually have a series of beams and purlins, with south-facing solar modules in northern latitudes. Most fixed-tilt racks in North America have tilt angles from 10 to 30 degrees. *Single-axis trackers (SATs)* usually have a torque tube oriented from north to south, with a motor and gear drive such that each rack tracks the path of the sun throughout the day from east to west. The torque tubes pass through a series of bearings such that they are free to rotate outside of the gear drive. Most SATs include a stow strategy to reduce angle of attack above a certain detected wind speed threshold. *Dual-axis trackers* are usually mounted on a mono-pole, and track the sun path such that the modules are continuously oriented toward the sun. Dual-axis trackers and parking lot canopy structures are outside the scope of this paper.

Modules can be arranged on a rack mounting system in *portrait* or *landscape*, and can be single rows or multiple rows, depending on the configuration of the rack. For example, most single-axis trackers have a single row of modules in portrait, attached to the torque tube by rails. Fixed-tilt racks will have multiple rows of modules in portrait or landscape. For fixed-tilt rack systems, a distinct portion of an array that is structurally independent of adjacent racks is referred to as a *table*. For example, in industry jargon, one might describe one table as "2Px10" to describe a rack "two high in portrait" by 10 modules wide. If one were to lay a measuring tape over the top of a table, the distance from the lowest edge to the highest edge can be referred to as the *chord length*, as shown in Figure 2.

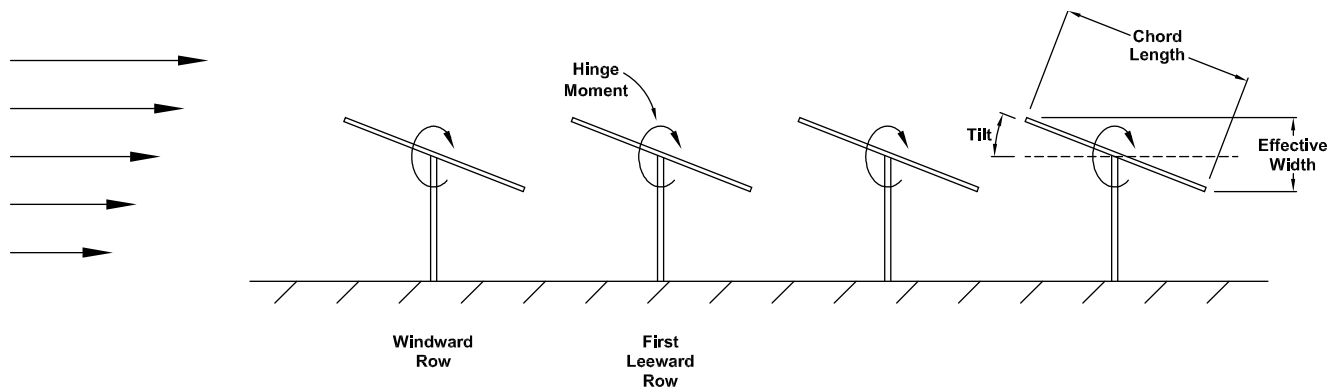


Figure 2: Simplified PV rack system geometry and terminology

## Wind Loads from ASCE 7

### Wind Speed

From ASCE 7-10 Table 1.5-1, Risk Category (RC) is usually assigned as Risk Category I (one), as ground-mounted rack systems are non-building structures that typically represent a low risk to human life in the event of failure. Therefore, wind speeds are usually found in ASCE 7-10 Figure 26.5-1C for Risk Category I. Readers of the 2012 International Building Code (IBC) or 2013 California Building Code (CBC) have on occasion interpreted Table 1604.5 as requiring RC III or even RC IV owing to a "shopping list" that includes "power generating stations." Risk categories III and IV do not apply, as they are intended to avoid interruption of electricity to critical infrastructure following a high wind event. This added level of reliability appears unnecessary for a solar power plant where production is interrupted nightly.

Where the locations of solar power plants fall within or near Special Wind Regions identified in ASCE 7, the reader is cautioned to carefully consider other data for local design wind speed. Recent site-specific wind studies for solar power plants have identified room for improvement in the boundaries of mapped Special Wind Regions in ASCE 7, and in the design wind speeds provided by local building departments. The commentary of ASCE 7 indicates that "some" of the special wind regions are shown in their wind maps, but does not preclude the existence of others that have not yet been identified. Many PV power plants are being built in remote regions that did not receive much scrutiny in the development of the current wind maps.

### Wind load coefficients

Even though ground-mounted PV rack systems are non-building structures, the net pressure coefficients for monoslope free roofs from ASCE 7 provide reasonable (though not necessarily conservative) wind loads in most cases. The wind pressures on individual panels – and therefore the mounting clamps or fasteners that attach the

panels to purlins – are most accurately derived from Chapter 30, Wind Loads on Components and Cladding (C&C). For the primary structure, the MWFRS Directional Procedure of Chapter 27 for Wind Loads on Buildings is the most common method used to determine wind pressures directly from ASCE 7. In this method, Net Pressure Coefficients  $C_N$  are found in Figure 27.4.4 for Monoslope Free Roofs.

The code provides a Gust Effect Factor  $G$  of 0.85 for rigid structures, and then advises that low-rise structures are permitted to be considered rigid. As with the rest of ASCE 7-10, the authors of this standard did not envision it being applied to utility-scale PV plants. Both parts of this are not suitable for the kind of racking systems we are addressing in this study. As we will see later, these structures are often not functionally rigid (meaning stiff enough to avoid dynamic effects), and even if they were, a gust effect factor of 1 is more appropriate for structures this small. Our advice is to set  $G = 1$  and then ignore it. The next paragraph provides our rationale for those interested.

The gust effect factor was introduced in its current form in ASCE 7-95, and the genesis is well-explained by its creators, Solari and Kareem (1998). The goal is to account for the fact that a 3-second gust will not completely envelope and simultaneously load all sides of a building. When calculating loads on the MWFRS using mean pressure coefficients on the building envelope, the 3-second gust wind speed is too short a duration for the building to fully respond. For a structure that is only 2 meters wide, a 3-second gust is more than long enough in duration to completely load the MWFRS. At 90 mph (40 m/s), a 3-second gust is 60 times larger than the structure. It is closer to a point structure. Here we quote directly from Solari and Kareem:

“If a structure is infinitely rigid and small, the non-contemporaneous action of wind and resonant effects are negligible and  $G = 1$  ... implying that the equivalent static pressure  $p$  is simply the product of the peak dynamic pressure and the [mean] pressure coefficient.”

In fact, if mean pressure coefficients are to be used, then a value of  $G > 1$  is more appropriate for a structure of this size.

Rather than attempting to factor or adjust the gust wind speed pressure in order to use mean pressure coefficients, it is easier to directly measure the correlated load on the structure in the wind tunnel and normalize it by the 3-second gust wind speed. This is what was done to derive the  $GC_p$  cladding pressure coefficients in the code.

### Atmospheric Boundary Layer Wind Tunnel Studies

Many manufacturers of rack mounting systems for utility scale PV systems have considered wind tunnel studies to be an important part of their value engineering. Resultant static

wind pressure coefficients are often lower than the tabled values found in ASCE 7, particularly in the array interior. By commissioning wind tunnel studies, manufacturers can reduce both construction cost and risk of structural failure by incorporating better understanding of wind pressures into their design practice to optimize their designs.

Wind tunnel studies for large-scale ground-mounted PV rack mounting systems are performed using a scale model of the rack system (often in approximately 1/50 scale) in a boundary layer wind tunnel, according to the Wind Tunnel Procedure described in ASCE 7-10 Chapter 31. Upwind surface roughness effects are simulated with objects placed upstream in the wind tunnel. A scale model is constructed to represent the geometry of the tables, including tilt angle, chord length, and the height of the lowest edge above the ground surface. As shown in Figure 3, the rows of tables are placed on a turntable inside the wind tunnel, such that wind effects can be measured from a full range of approach angles. Pressure taps are installed in the tables to record pressure data at very high frequencies (on the order of 500 Hz).

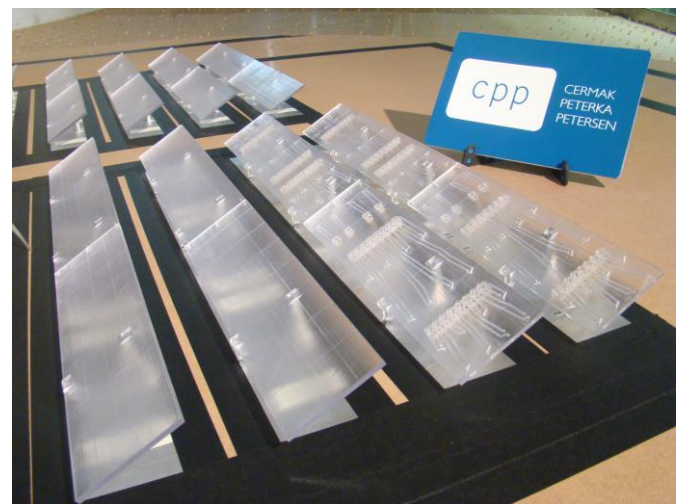


**Figure 3: Scale model of PV system on turntable in wind tunnel, showing pressure taps**

Different static pressure coefficients are often provided for portions of the array. The boundaries of the arrays are unsheltered from wind, with highest static wind pressures in array corners, then north and south edge rows, and east and west edge tables. The lowest static wind pressures are seen in the interior of the arrays owing to sheltering from wind by surrounding tables.

As described above, a proper *atmospheric boundary layer* (ABL) wind tunnel simulation will provide a combined net gust pressure coefficient across the modules,  $GC_N$ . Tests are sometimes inappropriately conducted at full scale in smooth-

flow aerospace wind tunnels, resulting in mean pressure coefficients, which then need to be adjusted using a suitable gust effect factor. This is not recommended for a host of reasons, not the least of which is because the loads are generally not quasi-steady and even the mean pressure coefficients can be incorrect. The mean wind load is not a reliable predictor of the peak wind load. Some of the low-rise wind loads in ASCE 7-10 date from the ANSI 1972 standard, when using mean load was often the only option due to the data collection limitations and measurement methods of the time. In 2015, there is no compelling reason to avoid direct measurement of peak wind loads.

In Figure 4, we compare net uplift and downforce on the perimeter of the array from ABL wind tunnel test data for various ground mount configurations with the values from the ASCE 7 monoslope free roof table, with  $G = 1$ . The scatter in the wind tunnel data is the result of different tributary areas (shorter or longer spans associated with a single support post), ground clearances, and row-to-row spacing. In some cases, the support structures themselves affect the flow beneath the modules.

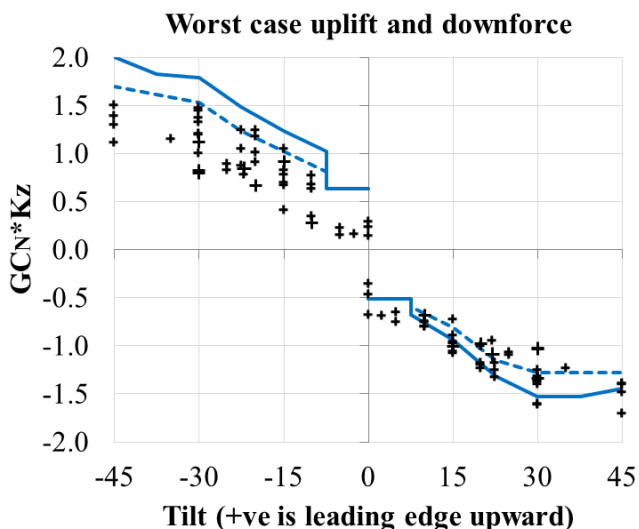


**Figure 4: Comparison of wind tunnel data from ground mount racking system studies with ASCE 7 values. (ASCE 7 curves were calculated with a value of  $G = 1.0$  and  $K_z = 0.85$ . Negative  $GC_N$  is uplift.)**

In Figure 4, the ASCE 7 balanced load case (Case A) is shown as a solid line, the unbalanced (Case B) as a dashed line. In general, the balanced load cases can be seen to envelope the data, with the exception of uplift at low tilt angles. However, the load patterns provided in Case A – which sometimes feature higher loads on the leeward side – were never observed during any of the testing. Peak row-end cantilever moments are not captured by the top-half/bottom-half load patterns in the code. These unbalanced patterns do

not accurately reflect some load distributions. For example, they will not properly predict top-of-post moments for single rows of posts supporting off-center tables. This is not surprising, as the loads in ASCE 7 have only been validated for small carports with corner supports (Uematsu et al, 2007).

The peak loads shown in Figure 4 were not all measured in the first windward row. In some cases, the data points are for the last leeward row, and other data points are for the second row. The presence of rows of racks behind and beside the table has a significant effect on the loads. Given that the ASCE 7 coefficients are from short-aspect-ratio tests of isolated tables, it is remarkable that the monoslope free roof values match the data as well as is shown.

When visualizing the wind flow over the array in the wind tunnel, one of the most obvious effects is the separation of the wind over the first row, followed by a reattachment near the second row. When the shear layer comes down directly on the second row, the peak wind loads rival those in the first row. This shear layer is quite unsteady. When examining the wind loads in the second row, it is apparent that there is a spike in energy of the kind typically associated with vortex shedding. This effect has only recently been apparent at solar PV power plants, as a result of forensic analysis to determine the cause of failure of code-compliant structures.

### Vortex Shedding

Vortex shedding – often referred to as *Von Kármán Vortex Street* – is a naturally occurring phenomenon, as seen in cloud cover near an island in Figure 5. An example of a computational fluid dynamics (CFD) model is shown in Figure 6. Vortex shedding creates cycles of alternating pressure on a fixed object in the wake.



**Figure 5: Naturally occurring Von Kármán vortex shedding downstream from island**

The Von Kármán vortex street is well understood by the wind engineering community and experts of fluid dynamics. It is typically described by the fixed Strouhal number,  $St$ , at which the vortices are shed from any given shape.

$$St = fL/U \quad (1)$$

where  $f$  is the frequency in Hz,  $L$  is the characteristic length of the body, and  $U$  is the wind speed in m/s. In this case,  $L$  is the vertical projection of the chord length,  $C$ , and is given by:

$$L = C * \sin(\theta) \quad (2)$$

where  $\theta$  is the tilt angle of the table. For SATs, tilt angle  $\theta$  is variable. Since  $St$  is fixed for any given shape, if the wind speed is doubled, the frequency of the vortex shedding is also doubled. Equation (2) also implies that the vortex shedding frequency increases for lower tilt systems.

The expected value of  $St$  for a tilted flat plate is 0.15 (Fage & Johansen, 1927) or 0.16 (Chen and Fang, 1997). Note that Equation (2) is not accurate for tilt angles less than about 10 degrees, as the vortex shedding energy peak is less well predicted by vertical projected height.

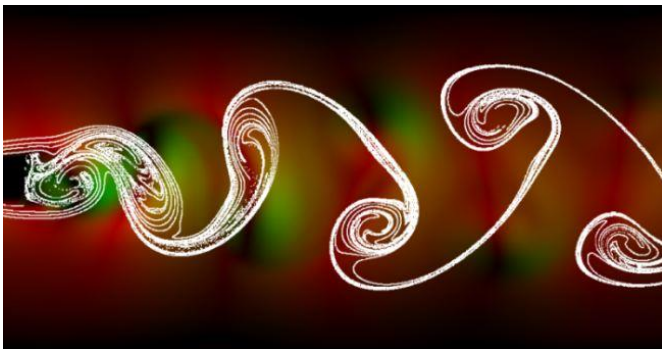


**Figure 6: Computational Fluid Dynamics (CFD) model of Von Kármán vortex street**

A fixed-tilt ground mount is typically arranged close to the ground in arrays with multiple rows. The winds approaching the array near the ground are quite gusty, and are even more gusty inside the array. All of these factors act to prevent the kind of “clean,” reliably spaced vortex shedding seen in the figures above. In some ways, this makes things worse. The peak in energy is still there, it is just spread out over a wider range of frequencies. Rather than worrying that one of your system’s natural frequencies may occasionally perfectly match  $f_s$ , you now need to be concerned when any of them are in the same ballpark.

During a storm with a 50 m/s (115 mph) wind gust at a height of 10 m in open country, we expect the hourly mean wind

speed at panel height will be about 25 m/s. Assuming  $St = 0.15-0.16$ , if the racking system has a chord length of 4 m (for example, 2 high in portrait) and a tilt angle of 20°, then Equation (1) indicates that it will shed vortices at 3 Hz. If the racking system has a natural frequency of 3 Hz, it is perfectly tuned for dynamic excitation.

As it is the wake of the upwind panels that causes this problem, interior rows of panels are more susceptible to dynamic issues than panels on the array perimeter.

Studies have shown the energy associated with vortex shedding for a ground mount system typically has a big peak near  $St \sim 0.12$ , and the peak usually drops off significantly for  $fL/U > 0.2$ . This is illustrated in the energy spectrum in Figure 7.

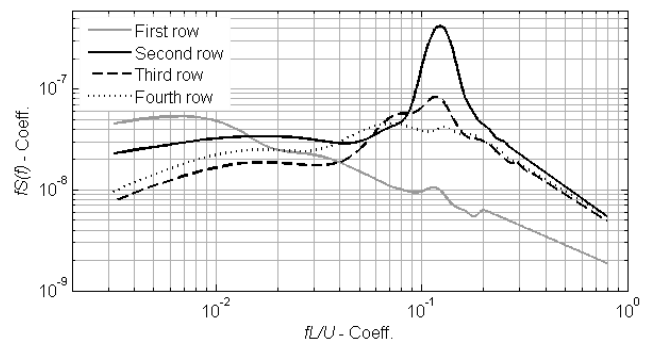


**Figure 7: Energy Spectrum vs. reduced frequency ( $fL/U$ )**

### Rigid versus Flexible Structures

ASCE 7-10 Section 26.2 defines “Building or Other Structures, Rigid” as: “A building or other structure whose fundamental natural frequency is greater than or equal to 1 Hz.” Section 26.2 also defines “Building and Other Structure, Flexible” as: “Slender buildings and other structures that have a fundamental natural frequency less than 1 Hz.”

As the Strouhal calculations and data above make clear, the 1 Hz threshold was never intended for use with structures as small as individual solar panels, and certainly not row-upon-row of them. The 1 Hz threshold is intended for building structures such as air traffic control towers and skyscrapers.

For the system described above, a better initial threshold for avoiding the worst dynamic effects would be a natural frequency greater than about 4 or 5 Hz, a rule of thumb that is sometimes applied for systems of this type. This threshold would increase if the design wind speed increased, if the tilt angle was reduced, or if the chord length was smaller. The initial threshold could decrease for other rack geometries.

Note that keeping reduced frequencies  $fL/U$  greater than 0.2 does not guarantee that dynamic effects will be negligible. In some situations, the wind excitation energy at reduced frequencies above 0.2 is not negligible, and analysis is needed to show that the structure can handle the inertial loads associated with modal excitation.

ASCE 7, like most wind loading standards around the world, does recognize this possibility. Section 27.1.2 allows use of this equivalent static force (ESF) wind loading method if:

“The building does not have response characteristics making it subject to across-wind loading, *vortex shedding*, instability due to galloping or flutter; or it does not have a site location for which channeling effects or buffeting in the wake of upwind obstructions warrant special consideration.”

Section 26.9.5 of ASCE 7-10 includes a method for considering flexible or dynamically sensitive structures. This is used to adjust the gust effect factor, which is designed to capture the along-wind response of the structure due to different gust durations in the approaching wind. These formulas provide no method for taking into account the big spike in gust wind energy due to vortex shedding, and they should not be used. As with the static loads, the gust effect factor  $G$  should be set to 1.0 and ignored.

So what can be done to determine the loads associated with modal excitation due to this broadband vortex shedding? While the natural frequencies are different than skyscrapers, the analysis needed is identical, and is well-established. The first step is to examine the modes of vibrations.

## Modal Analysis and Natural Frequency

Most Finite Element Analysis (FEA) applications are capable of providing *modal analysis* to determine critical mode shapes and their associated natural frequencies of vibration. This is sometimes referred to as *Eigenvalue Analysis*. The accuracy of FEA modal analysis is highly dependent on assumptions used when building the FEA model. For example, PV modules are often mounted to purlins using module clamps or bolts at four distinct points. Modeling all PV modules within one table as a continuous plate would over-estimate the stiffness of the table. Modeling the PV modules with connections at four distinct points (that is, at module clamp locations) is more tedious. The accuracy of the FEA model is also influenced by assumptions for joint fixity.

For ground-mounted systems, assumptions for steel piles are very important. For example, a common error is to model the steel piles as *fixed* at the soil surface. If soil conditions are known or assumed, a more-complex model can be developed using soil springs along the embedment depth of steel piles.

As an alternative, an approximation can be developed using a point of fixity at some depth below the soil surface. If further study is needed, the ideal case would be to first perform field vibration testing (as described in the next section), then calibrate the FEA modal analysis model (for example, point of pile fixity below ground surface) to obtain the same resultant natural frequencies as in field testing.

The goal of modal analysis is to identify the mode shapes with lowest natural frequencies that can be excited by wind. Common mode shapes of concern for a fixed-tilt mounting system are inverted pendulum sway in the north-south direction and in the east-west direction. Often there will be a family of these modes. For example, a table with two center posts might have both posts sway in unison, and 180 degrees out of phase.

Note that for a fixed tilt system facing south (or north in the southern hemisphere), the east-west sway mode is difficult for the wind to excite, because the vast majority of the wind pressure acts across the PV modules (from top-to-bottom). This thought process can be applied to all mode shapes – for significant wind excitation, there needs to be modal motion normal to the plane of the PV tables.

A second family of modes common to both single-axis trackers and fixed-tilt systems, is up-and-down motion in-between the posts. Again, there will often be a family of these modes, with neighboring post-to-post spans moving in phase or out of phase. By their very nature (heaving up and down), these primarily involve motion normal to the plane of the tables, and so are quite susceptible to wind excitation.

The lowest frequency mode for SATs is almost always torsion about the torque tube, with the greatest angular displacement at the row ends, and minimal angular displacement near the drive motor or drive shaft. The modes are almost always at frequencies below 2 Hz. Using the guidelines above, we can see that this torsional mode can be excited at wind speeds below the typical detected stow velocities of 40-60 mph.

## Dynamic Analysis

Dynamic analysis is traditionally conducted in the frequency domain using a mechanical admittance function, as described in Guha et al (2015). An approximate analysis can be performed for a single mode by assuming that the effects of a given mode directly correspond (1:1) to a static load coefficient of concern (for example, where motion in the north-south sway mode is considered to translate directly into increased base moments). The output from such an analysis is often presented as a *dynamic amplification factor*, or DAF, which is a multiplier (always greater than 1.0) to be applied

to the static loads which will predict the combined static and dynamic loading.

The sample DAF plot in Figure 8 is for a particular interior row mode shape. The peak DAF is 2, which will typically offset all of the static load reductions from a wind tunnel study of loads in the array interior. This can be avoided by keeping the natural frequencies and/or damping ratios high enough. The DAF can be considerably higher for the second row, sometimes greater than 5 at the peak  $fD/U$ . Note that the DAF is greater than 1.0 at  $fD/U = 0.2$ . ( $D = L$  in this case.)

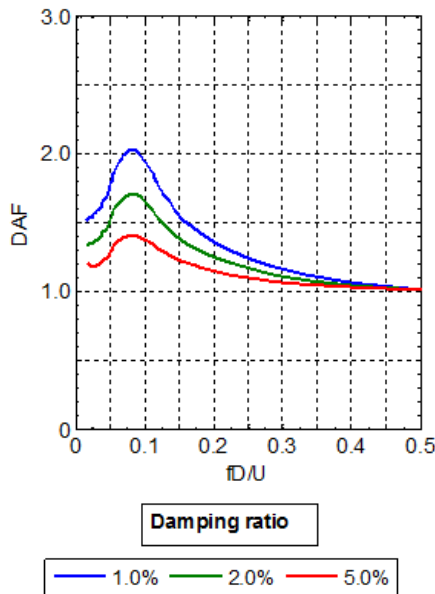


**Figure 8: Dynamic Amplification Factor (DAF) for a single mode shape for interior rows.**

The most precise method is to include all modes of concern in the frequency domain, and determine the effect of a particular component using modal influence coefficients. A similarly precise method is to conduct the dynamic analysis by inputting the time series of wind excitation into the FEA software. The wind tunnel time series data needs to be of sufficient duration that the effects of buffeting from vortex shedding can be statistically characterized. This generally means running the simulation for a few minutes of full scale winds. The point of diminishing return will be evident.

Note that because of the unusually large model scales required for ABL wind tunnel tests of ground mounted solar, if this is the source of the time series, then the wind tunnel must provide some method of compensating for missing low frequency turbulence (Banks et al 2015, Mooneghi et al. 2015). A DAF can be determined by turning off the mass to obtain the background response, then statistically comparing the peaks from each method.

Figure 8 illustrates that the effects of dynamic loading induced by vortex buffeting depend significantly on the damping ratio. If the damping ratio is below 1%, small (2 m chord length) ground mounted systems with natural frequencies under 2 Hz can experience dynamic loads that are 2-10 times greater than the static loads. Failures are often not as evident as with rooftop PV systems, since the ground mounted panels will probably still be where they were placed. However, post-storm inspection would reveal the beginning of plastic deformation of structural components and connections. Anyone watching the array during the storm would not miss the swaying and/or twisting of the rack systems that caused the damage. This effect will be most pronounced in the second upwind row.

In some cases, systems will have significant damping, for example due to single-axis tracker drive motors or aerodynamic damping. This will keep the motion from becoming excessive. Add-on damping systems (similar in appearance to automotive shock absorbers) can also be incorporated into the design of SATs.

### Field Vibration Testing of Built PV Rack Systems

The most definitive way to understand the vibration behavior of ground-mounted PV rack systems (and the only way to accurately determine the damping ratio) is to conduct field vibration testing of built systems. These tests include interaction of all components of the system from PV module stiffness and attachment method, true behavior of connections (which are usually somewhere in-between *fixed* and *pinned*), and characteristics of foundation piles with soil interaction. As vibration behavior is dependent on foundation type and member selection as well as soil characteristics, results from off-site prototyped systems can be significantly different from field results for a particular built project.

In the most pure form, the system is displaced and then suddenly released and allowed to vibrate freely. This is sometimes referred to as a “pluck test,” which is effective for some mode shapes but not all. Some mode shapes are more easily excitable with human effort. However, with human effort it is sometimes not possible to isolate only one mode shape, as other sympathetic mode shapes can be activated.

In professional field vibration testing, accelerometers are mounted to the PV tables in strategic locations. Use of accelerometers is ideal, as the damping ratios of various mode shapes can be equally significant in the determination of DAFs. Professional vibration study reports include a clear description of each mode shape along with its natural frequency and damping ratio.

The most rudimentary method of field vibration testing involves taking video recordings of motion using human effort to excite the various mode shapes. In this method, it is best to use a tripod for the video recording device. When viewing playback of the video, it is necessary to know the number of frames per second (often 29 frames per second in modern devices). The natural frequency of each excitable mode shape can be determined by pausing the video and then counting mouse clicks to advance the video one frame at a time through one complete vibration cycle.

The damping ratio is very difficult to determine using this visual method without accelerometers, as the decay in amplitude is difficult to quantify from a video. It is possible to obtain limited information at lower cost using the accelerometer built into many smart phones. This shortcut method still allows rough determination of damping ratios based on Fast Fourier Transforms (FFTs) in addition to natural frequencies. Results are generally less conclusive than professional studies, unless multiple accelerometers are used in meaningful locations.

## Conclusions

Ground mounted solar racks with natural frequencies above 1 Hz should not be considered rigid. For many fixed tilt systems, a natural frequency of 2 Hz is perfectly tuned to maximize dynamic effects in a design wind event. A better frequency limit can usually be estimated by ensuring the reduced frequency,  $fL/U$ , is greater than 0.2. However, for some mode shapes, we have seen DAF values greater than 1.3 for  $fL/U$  above 0.2.

A better initial threshold for typical ground mounted systems with 4 m chord is 4 or 5 Hz, to avoid maximum amplification of load owing to frequency matching. However, it is important to understand the vortex shedding frequency varies with rack geometry and wind speed. A single frequency threshold would be overly conservative for many PV rack structures, and this value may not be high enough in high wind environments or for smaller structures at lower tilts.

The gust effect factor  $G$  in ASCE 7 should be set to 1.0 for the kinds of racking systems examined in this study, and should not be used to account for dynamic sensitivity effects on these structures.

Use of the monoslope free roof static loads from ASCE 7 provides reasonable predictions for some load effects on ground mounted single-axis trackers, though the loading patterns are often unrealistic.

Dynamic analysis on utility scale solar racking products can be (and should be) conducted using methods developed for

tall slender structures. Dynamic amplification factors greater than 2 are not uncommon for systems with damping ratios less than 2% of critical damping. Damping ratio must be measured on built systems in the field.

## References

American Society of Civil Engineers, *Minimum Design Loads for Buildings and Other Structures* (ASCE 7-10), 2010.

Banks, D., Guha, T, and Fewless, Y., "A hybrid method of generating realistic full-scale time series of wind loads from large-scale wind tunnel studies: Application to solar arrays," proceedings of the 2015 International Conference on Wind Engineering, Porto Alegre, Brazil.

Chen, J.M., and Fang, Y., "Strouhal numbers of inclined flat plates," *Journal of Wind Engineering and Industrial Aerodynamics*, 61 (1996) 99-112.

Fage, A. and Johansen, F.C., "On the flow of air behind an inclined flat plate of infinite span", *Proceedings of the Royal Society of London*, 116 (1927) 170-197.

GTM Research/Solar Energy Industries Association, *U.S. Solar Market Insight: 2014 Year-in-Review*, March 10, 2015.

Guha, T, Fewless, Y., and Banks, D., "Effect of panel tilt, row spacing, ground clearance and post-offset distance on the vortex induced dynamic loads on fixed tilt ground mount photovoltaic arrays," proceedings of the 2015 International Conference on Wind Engineering, Porto Alegre, Brazil.

Mooneghi, M.A, Irwin, P., and Chowdhury, A.G, "Partial Turbulence Simulation Method for Small Structures," *Proceedings of the 2015 International Conference on Wind Engineering*, Porto Alegre, Brazil.

Solari, G., and Kareem, A., "The formulation of ASCE 7-95 gust effect factor," *Journal of Wind Engineering and Industrial Aerodynamics*, 1998, Vol. 77&78, 673-684.

Strobel, K. and Banks, D., "Effects of Vortex Shedding in Arrays of Long Inclined Flat Plates and Ramifications for Ground-mounted Photovoltaic Arrays," *Journal of Wind Engineering and Industrial Aerodynamics*, 2014, Vol. 133, 146-149.

Uematsu, Y., Izumi, E., and Stathopoulos, T., "Wind Force coefficients for designing free-standing canopy roofs," *Journal of Wind Engineering and Industrial Aerodynamics*, 2007, Vol. 95, 1486-1510.